J|A|C|S
ARTICLES
Published on Web 09/15/2005

Heterometallic Chalcogenido Clusters Containing Lanthanides and Main Group Metals: Emissive Precursors to Ternary Solid-State Compounds

Anna Kornienko,[†] Santanu Banerjee,[†] G. Ajith Kumar,[‡] Richard E. Riman,[‡] Thomas J. Emge,[†] and John G. Brennan*,[†]

Contribution from the Department of Chemistry and Chemical Biology, and Department of Materials Science and Engineering, Rutgers, the State University of New Jersey, 610 Taylor Road, Piscataway, New Jersey 08854-8087

Received May 27, 2005; E-mail: bren@ccbmail.rutgers.edu

Abstract: Heterometallic clusters containing lanthanides and the group 12 metals can be isolated as crystalline compounds in high yields. These products $[(py)_8Ln_4M_2Se_6(SePh)_4$ (Ln = Er, Yb, Lu; M = Cd, Hg)] adopt a double cubane structure with the covalent M occupying an opposing pair of external metal sites. Both Er/M compounds are strongly emissive materials, with emission lifetimes of 1.41 ms (Er/Cd) and 0.71 ms (Er/Hg) and with the Er/Cd radiative quantum efficiency twice that of the Er/Hg compound. Thermal decomposition of the Er/Cd and Yb/Cd compounds at 650 °C give the ternary solid-state materials $CdLn_2Se_4$.

Introduction

Emission of light from lanthanide ions is a fundamentally important process with a continuously expanding range of applications in contemporary electronic devices, from TV screens to lasers and optical fibers.[1−5] Control of emission intensity is often elusive, with competitive processes such as upconversion, photon splitting, or nonradiative (vibronic) quenching often detracting from ideal performance.[6] Air-stable oxide-based materials dominate most current applications that employ Ln emission, with methods for incorporation of Ln into these materials being relatively facile and straightforward. Emerging, non-oxide-based materials (i.e., organic polymers, sulfide glasses) can also exploit the unique properties of Ln emissions, and these relatively uncharted areas require new approaches to the delivery and incorporation of Ln ions.

Considerable effort has been devoted to the chemistry of Er compounds that might be useful for amplifying optical fiber signals with emission at 1.54 μm. Numerous reports describe the preparation of perfluorinated compounds that enhance Er emission by minimizing the presence of C−H functional groups that vibronically quench[7−12] the emissive Er $^4I_{13/2}$ excited state.[13,14] An alternative method for enhancing Er emission involves tethering strongly absorbing ligands that transfer energy[15,16] to Er and thus increase the population of the $^4I_{13/2}$ state. Most recently, Er compounds with chalcogen-based anions were found to exhibit long excited-state lifetimes and intense emission properties. The nanoscale cluster $(THF)_{14}Er_{10}S_6(SeSe)_6I_6$ (Er_{10}) was first shown to emit 1.54 μm light with a 78% quantum efficiency,[17] and this report was followed by a comparison between the Er_{10} cluster and the fluorinated thiolate complex $(DME)_2Er(SC_6F_5)_3$.[18] High emission intensities were attributed to absence of strongly bound ligands with C−H or O−H bonds within the primary Er coordination spheres. Significantly, while the Er thiolate maintained its emission properties when doped into a fluorinated polymer matrix, the Er_{10} cluster compound did not.[19]

[†] Department of Chemistry and Chemical Biology.
[‡] Department of Materials Engineering.

(1) Silversmith, A. J.; Lenth, W.; Macfarlane, R. M. *Appl. Phys. Lett.* **1987**, *51*, 1997.
(2) Maciel, G. S.; de Arajuo, C. B.; Massaddeq, Y.; Aegerter, M. A. *Phys. Rev. B* **1997**, *55*, 6335.
(3) Hebert, T.; Wannermacher, R.; Lenth, W.; Macfarlane, R. M. *Appl. Phys Lett.* **1990**, *57*, 1727.
(4) Dowing, E.; Hesselink, L.; Ralston, J.; Macfarlane, R. M. *Science* **1986**, *273*, 1185.
(5) Bhargava, R. N.; Gallaghar, D.; Hong, X.; Nurmikko, A. *Phys. Rev. Lett.* **1994**, *72*, 416.
(6) DiBartolo, B., Ed. *Spectroscopy of Solid State Laser Type Materials*; Plenum Press: New York, 1987.
(7) Hebbink, G. A.; Reinboudt, D. N.; van Veggel, F. C. J. M *Eur. J. Org. Chem.* **2001**, *4101*.
(8) Sloof, L. H.; Polman, A. *J. Appl. Phys.* **1998**, *83*, 497.
(9) Wolbers, M. P. O.; van Veggel, F. C. J. M.; Snellink-Ruel, B. H. M.; Hofstraat, J. W.; Geurts, F. A. J.; Reinhoudt, D. N. *J. Am. Chem. Soc.* **1997**, *119*, *138*.
(10) Wolbers, M. P. O.; van Veggel, F. C. J. M.; Peters, F. G. A.; van Beelen, E. S. E.; Hofstraat, J. W.; Geurts, F. A. J.; Reinhoudt, D. N. *Chem. Eur. J.* **1998**, *4*, 772.
(11) Hasegawa, Y.; Okhubo, T.; Sogabe, K.; Kawamura, Y.; Wada, Y.; Nakashima, N.; Yanagida, S. *Angew. Chem., Int. Ed.* **2000**, *39*, 357.
(12) Kumar, G. A.; Ballato, J.; Snitzer, E.; Riman, R. E. *J. Appl. Phys.* **2004**, *95*, 40.
(13) Kaminskii, A. A. *Laser crystals-Their Physics and Properties*; Springer-Verlag; New York, 1990.
(14) Becker, P. C.; Olsson, N. A.; Simpson, J. R. *Erbium Doped Fiber Amplifiers-Fundamentals and Technology*; Academic Press: New York, 1999.
(15) Wang, H.; Qian, G.; Wang, M.; Zhang, J.; Luo, Y. *J. Phys. Chem. B* **2004**, *108*, 8084.
(16) Hofstraat, J. W.; Wolbers, M. P. Oude; Van Veggel, F. C. J. M.; Reinhoudt, D. N.; Werts, M. H. V.; Verhoeven, J. W. *J. Fluoresc.* **1998**, *8*, 301.
(17) Kornienko, A.; Kumar, G. A.; Riman, R. E.; Emge, T. J.; Brennan, J. G. *J. Am. Chem. Soc.* **2005**, *127*, 3501.
(18) Kumar, G. A.; Riman, R. E.; Torres, L. A. D.; Garcia, O. B.; Banerjee, S.; Kornienko, A.; Brennan, J. *Chem. Mater.* **2005**, *17*. In press.

10.1021/ja0534708 CCC: $30.25

The chemistry of chalcogenido compounds containing both Ln and main group metals has been a synthetic challenge motivated by a range of applications, from optical fibers,[20−23] doped semiconductors,[24−26] and LEDs[27−30] to nanocluster fluorescence labels.[31−34] While there exist numerous descriptions of emissive lanthanide/semiconductor materials in the literature, there still exists no clear molecular picture of the manner in which Ln and M both interact with E^{2-} ligands. Recent cluster work has demonstrated that complications can arise when attempting to prepare materials with Ln−E−M connectivity. For example, structural characterization of the ionic compound $[Yb(THF)_6][Fe_4Se_4(SePh)_4]$[35] revealed that the more covalent metal can completely abstract all chalcogen electron density from the Ln coordination sphere. A similar abstraction was noted in $[(THF)_8Sm_4Se(SePh)_8][Zn_8Se(SePh)_{16}]$. This ionic heterocluster material is particularly thought provoking because, although spectroscopic methods might correctly indicate the presence of Sm−Se^{2-} bonds and Zn−Se^{2-} bonds, the compound contains no Sm−Se−Zn connectivity.[35] From these studies it became clear that M:Ln ratios greater than 1:1 were particularly deleterious to the goal of isolating discrete compounds with Ln−E−M linkages.

If Ln−E−M systems are to be developed, either as emissive materials or as precursors to solid-state Ln-doped semiconductors, a detailed understanding of the molecular chemistry leading up to, and physical properties of, compounds with Ln−E−M linkages is required. This contribution outlines syntheses of the first molecular examples of compounds with structurally characterized Ln−E^{2-}−M linkages. Once formed, this connectivity is shown to be chemically robust, and the utility of these compounds in the synthesis of ternary solid-state materials is demonstrated. Further, the near-IR emission properties of the Er compounds are described, and correlations of structure with emission intensity are drawn.

Experimental Section

General Methods. All syntheses were carried out under ultrapure nitrogen (Airtech), using conventional drybox or Schlenk techniques. Solvents (Fisher) were refluxed continuously over molten alkali metals or K/benzophenone or purified in a double-column solvent purification system (Solvtech) and were collected immediately prior to use. Anhydrous pyridine (Aldrich) was purchased and refluxed over KOH. Ln were purchased from Strem. PhSeSePh was purchased from Aldrich and recrystallized from hexane. Melting points were taken in sealed capillaries and are uncorrected. IR spectra were taken on a Mattus Cygnus 100 FTIR spectrometer, and recorded from 4000 to 600 cm^{-1} as a Nujol mull on NaCl plates. Electronic spectra were recorded on a Varian DMS 100S spectrometer with the samples in a 0.10 mm quartz cell attached to a Teflon stopcock. Powder diffraction spectra were obtained from Bruker AXS D8 Advance diffractometer using Cu Kα radiation. Elemental analyses were performed by Quantitative Technologies, Inc. (Whitehouse NJ).

Synthesis of $(py)_8Er_4Cd_2Se_6(SePh)_4$ (1). Cd (0.11 g, 1.0 mmol) and diphenyl diselenide (1.3 g, 4.0 mmol) were combined in pyridine (60 mL). The mixture was stirred until all the Cd was dissolved to give a yellow solution, then metallic Er (0.34 g, 2.0 mmol) and Hg (0.050 g, 0.25 mmol) were added. After 5 h the green solution was filtered from the drop of mercury. Elemental Se (0.16 g, 2.0 mmol) was added, the reaction mixture was stirred for 5 min, and then the yellow solution was filtered and layered with hexanes (2.0 mL) to give yellow needles (0.89 g, 68%) that do not melt but turn dark brown at 252 °C. Anal. Calcd for $C_{64}H_{60}Cd_2N_8Se_{10}Er_4$: C, 29.3; H, 2.30, N, 4.27. Found: C, 29.2; H, 2.31; N, 4.36. The compound does not show an optical absorption maximum from 300 to 800 nm in 4-ethylpyridine. IR: 3346 (s), 3169 (m), 2919 (w), 2727 (m), 2671 (m), 2406 (s), 2344 (s), 2180 (s), 2028 (s), 1911 (s), 1862 (s),1657 (s), 1639 (s), 1597 (m), 1579 (m), 1451 (w), 1377 (w), 1305 (m), 1262 (m), 1215 (m), 1168 (s), 1152 (m), 1079 (s), 1065 (m), 1030 (m), 1003 (s), 939 (s), 892 (s), 846 (s), 704 (m), 722 (w) cm^{-1}. Unit cell (Mo Ka, 100 K): $a = 12.952(1)$ Å, $b = 17.492(2)$ Å, $c = 17.086(2)$ Å, $\beta = 111.917(2)°$, $V = 3591.3(6)$ $Å^3$.

Synthesis of $(py)_8Er_4Hg_2Se_6(SePh)_4$ (2). Hg (0.20 g, 1.0 mmol) and diphenyl diselenide (1.3 g, 4.0 mmol) were combined in pyridine (50 mL). When all the Hg was consumed to give a yellow solution, metallic Er (0.34 g, 2.0 mmol) was added. In 12 h elemental Se (0.16 g, 2.0 mmol) was added to the deep-green solution. The reaction mixture was stirred for 5 min, filtered, and layered with hexanes (2.0 mL) to give yellow needles (1.1 g, 78%) that do not melt but turn brown at 185 °C and then black at 245 °C. Anal. Calcd for $C_{64}H_{60}Hg_2N_8Se_{10}Er_4$: C, 27.4; H, 2.16, N, 4.00. Found: C, 27.8; H, 2.66; N, 4.19. The compound does not show an optical absorption maximum from 300 to 800 nm in 4-ethylpyridine. IR: 3077 (m), 3023 (m), 2911 (w), 2726 (s), 2669 (s), 2608 (s), 2447 (s), 1978 (s), 1914 (s), 1863 (s), 1683 (s), 1631 (s), 1596 (m), 1580 (m), 1460 (w), 1438 (w), 1377 (m), 1300 (s), 1261 (s), 1233 (s), 1215 (m), 1182 (s), 1144 (m), 1068 (m), 1030 (m), 1001 (s), 991 (s), 745 (m), 703 (w) cm^{-1}.

Synthesis of $(py)_8Yb_4Cd_2Se_6(SePh)_4$ (3). Cd (0.11 g, 1.0 mmol) and diphenyl diselenide (0.94 g, 3.0 mmol) were combined in pyridine (60 mL). The mixture was stirred until all the Cd was dissolved to give a yellow solution, then metallic Yb (0.35 g, 2.0 mmol) and Hg (0.050 g, 0.25 mmol) were added. After 5 h the resultant black-purple solution was filtered from the drop of mercury, and elemental Se (0.16 g, 2.0 mmol) was added to the filtrate. The red-black mixture was stirred for 5

(19) Kumar, G. A.; Riman, R. E.; Chen, S.; Smith, D.; Ballato, J.; Banerjee, S.; Brennan, J. *Appl. Phys. Lett.* submitted.
(20) Allen, T. W.; Hawkeye, M. M.; Haugen, C. J.; DeCorby, R. G.; McMullin, J. N.; Tonchev, D.; Koughia, K.; Kasap, S. O. *J. Vac. Sci. Technol., A* **2004**, *22*, 921.
(21) Churbanov, M. F.; Scripachev, I. V.; Shiryaev, V. S.; Plotnichenko, V. G.; Smetanin, S. V.; Kryukova, E. B.; Pyrkov, Yu. N.; Galagan, B. I. *J. Non-Cryst. Solids* **2003**, *326/327*, 301.
(22) Borisov, E. N.; Smirnov, V. B.; Tverjanovich, A.; Tveryanovich, Yu. S. *J. Non-Cryst. Solids* **2003**, *326/327*, 316.
(23) Tonchev, D. T.; Haugen, C. J.; DeCorby, R. G.; McMullin, J. N.; Kasap, S. O. *J. Non-Cryst. Solids* **2003**, *326/327*, 364.
(24) Wruck, D.; Klimakow, A.; Rau, B.; Henneberger, F. *Semicond. Sci. Technol.* **2001**, *16*, 885.
(25) Hsu, Y.; Chang, C.; Hsieh, W. *Jpn. J. Appl. Phys., Part 1* **2003**, *42*, 4222.
(26) Konnov, V. M.; Loiko, N. N.; Sadof'ev, Yu. G.; Trushin, A. S. *Kratk. Soobshch. Fiz.* **2003**, *8*, 19.
(27) Hamano, F.; Tanaka, K.; Uchiki, H. *Jpn. J. Appl. Phys.* **2005**, *44*, 769.
(28) Kim, C.; Jang, K.; Lee, Y. *Solid State Commun.* **2004**, *130*, 701.
(29) Stouwdam, J. W.; Van Veggel, F. C. J. M. *ChemPhysChem.* **2004**, *5*, 743.
(30) Murphy, C. J.; Ellis, A. B. *J. Phys. Chem.* **1990**, *94*, 3082.
(31) Philipps, J. F.; Topfer, T.; Ebendorff-Heidepriem, H.; Ehrt, D.; Sauerbrey, R.; Borrelli, N. F. *Appl. Phys. B* **2002**, *74*, 285.
(32) Schmidt, T.; Mueller, G.; Spanhel, L.; Kerkel, K.; Forchel, A. *Chem. Mater.* **1998**, *10*, 65.
(33) Raola, O. E.; Strouse, G. F. *Nano Lett.* **2002**, *2*, 1443.
(34) Jose, G.; Jose, G.; Thomas, V.; Joseph, C.; Ittyachen, M. A.; Unnikrishnan, N. V. *Mater. Lett.* **2003**, *57*, 1051.
(35) Kornienko, A.; Huebner, L.; Freedman, D.; Emge, T.; Brennan, J. *Inorg. Chem.* **2003**, *42*, 8476.

Table 1. Summary of Crystallographic Details for **2**, **3**, and **4**

cmpd	**2**	**3**	**4**
empirical formula	$C_{64}H_{60}Er_4Hg_2N_8Se_{10}$	$C_{64}H_{60}Cd_2N_8Se_{10.1}Yb_4$	$C_{64}H_{60}Hg_2N_8Se_{10.08}Yb_4$
fw	2801.02	2656.05	2830.46
space group	$P2(1)/c$	$P2(1)/c$	$P2(1)/c$
a (Å)	12.9478(6)	12.8817(6)	12.9070(6)
b (Å)	17.5133(9)	17.4734(8)	17.5001(8)
c (Å)	16.9599(9)	17.0293(8)	16.9594(8)
β (deg)	111.879(1)	111.575(1)	111.894(1)
V (Å$^{3)}$	3568.3(3)	3564.5(3)	3555.5(3)
Z	2	2	2
D(calcd) (g/cm^{-3})	2.607	2.475	2.644
temp (K)	100(2)	100(2)	100(2)
λ (Å)	0.71073	0.71073	0.71073
abs coeff (mm^{-1})	14.079	10.983	14.713
$R(F)^a$ [$I > 2\sigma(I)$]	0.0416	0.0527	0.0415
$R_w(F^2)^a$ [$I > 2\sigma(I)$]	0.0978	0.1000	0.0843

[a] Definitions: $^aR(F) = \sum|F_o| - |F_c||/\sum F_o|$; $R_w(F^2) = \{\sum w(F_o^2 - F_c^2)^2]/\sum[w(F_o^2)^2]\}^{1/2}$. Additional crystallographic details are given in the Supporting Information.

min and then filtered and layered with hexanes (2.0 mL) to give orange crystals (0.99 g, 74%) that do not melt but turn dark brown at 224 °C. Anal. Calcd for $C_{64}H_{60}Cd_2N_8Se_{10}Yb_4$: C, 29.0; H, 2.28, N, 4.23. Found: C, 29.7; H, 2.35; N, 4.58. UV−vis (4-ethylpyridine): 410 ($\epsilon = 1.7 \times 10^3$) nm. IR: 3346 (s), 3169 (m), 2919 (w), 2727 (m), 2671 (m), 2406 (s), 2344 (s), 2180 (s), 2028 (s), 1911 (s), 1862 (s), 1657 (s), 1639 (s),1597 (m), 1579 (m), 1451 (w), 1377 (w), 1305 (m), 1262 (m), 1215 (m), 1168 (s), 1152 (m), 1079 (s), 1065 (m), 1030 (m), 1003 (s), 939 (s), 892 (s), 846 (s), 704 (m), 722 (w) cm^{-1}.

Synthesis of $(py)_8Yb_4Hg_2Se_6(SePh)_4$ (4). Hg (0.20 g, 1.0 mmol) and diphenyl diselenide (0.94 g, 3.0 mmol) were combined in pyridine (60 mL). The mixture was stirred until all the Hg was consumed to give a yellow solution, then metallic Yb (0.35 g, 2.0 mmol) was added. After 12 h, elemental Se (0.16 g, 2.0 mmol) was added to the black-purple solution. The reaction mixture was stirred for 5 min, and the red-black solution was filtered and layered with hexanes (2.0 mL) to give orange needles (1.1 g, 78%) that do not melt but turn dark brown at 235 °C. Anal. Calcd for $C_{64}H_{60}Hg_2N_8Se_{10}Yb_4$: C, 27.2; H, 2.14, N, 3.97. Found: C, 27.3; H, 2.19; N, 4.16. UV−vis (4-ethylpyridine): 410 ($\epsilon = 1.5 \times 10^3$) nm. IR: 3077 (m), 3023 (m), 2923 (w), 2726 (s), 2669 (s), 2608 (s), 2447 (s), 1978 (s), 1913 (s), 1860 (s), 1685 (s), 1637 (s), 1596 (m), 1579 (m), 1508 (s), 1463 (w), 1438 (w), 1377 (m), 1298 (s), 1262 (s), 1233 (s), 1216 (m), 1182 (s), 1145 (m), 1082 (s), 1067 (m), 1031 (m), 1001 (s), 941 (s), 890 (s), 820 (s), 745 (m), 703 (w) cm^{-1}.

Synthesis of $(py)_8Lu_4Hg_2Se_6(SePh)_4$ (5). Hg (0.20 g, 1.0 mmol) and diphenyl diselenide (1.3 g, 4.0 mmol) were mixed in pyridine (50 mL) and stirred until all the Hg was consumed to give a yellow solution, and then metallic Lu (0.35 g, 2.0 mmol) was added. After 12 h, elemental Se (0.16 g, 2.0 mmol) was added to the light-green solution. The reaction mixture was stirred for 5 min, filtered, and layered with hexanes (3.0 mL) to give yellow needles (0.94 g, 66%) that do not melt and stay yellow up to 300 °C. Anal. Calcd for $C_{64}H_{60}Hg_2N_8Se_{10}Lu_4$: C, 27.1; H, 2.14, N, 3.96. Found: C, 27.3; H, 2.25; N, 4.01. The compound is insoluble in THF or pyridine and does not show an absorption maximum in 4-ethylpyridine between 350 and 800 nm. IR: 3077 (m), 3023 (m), 2920 (w), 2710 (s), 2669 (s), 2608 (s), 2447 (s), 1985 (s), 1921 (s), 1841 (s), 1685 (s), 1633 (s), 1596 (m), 1574 (m), 1508 (s), 1455 (w), 1438 (w), 1372 (m), 1298 (s), 1262 (s), 1233 (s), 1216 (m), 1178 (s), 1152 (m), 1082 (s), 1064 (m), 1031 (m), 1001 (s), 939 (s), 898 (s), 842 (s), 732 (m), 692 (w) cm^{-1}.

Thermolysis and XRPD measurements. Cluster samples were placed in quartz tubes under vacuum and then sealed. The end of the tube with the sample was placed in an oven, the temperature was raised (20 °C/min) to 650 °C and held at this temperature for 5 h. The other end of the thermolysis tube was kept in liquid nitrogen during the experiment. Black powders formed, and powder diffraction patterns were obtained by scanning from 20 to 80°. The colorless liquid that condensed in the cold part of the tube was dissolved in acetonitrile and analyzed by GC/MS.

X-ray Structure Determination of 2, 3, and 4. Data for **2**, **3**, and **4** were collected on a Bruker Smart APEX CCD diffractometer with graphite monochromatized Mo Kα radiation ($\lambda = 0.71073$ Å) at 100 K. The data were corrected for Lorenz effects and polarization, and absorption, the latter by a multiscan (SADABS)[36] method. The structures were solved by Patterson or direct methods (SHELXS86).[37] All non-hydrogen atoms were refined (SHELXL97)[38] based upon F_{obs}^2. All hydrogen atom coordinates were calculated with idealized geometries (SHELXL97). Scattering factors (f_o, f', f'') are as described in SHELXL97. Crystallographic data and final R indices for **2**, **3**, and **4** are given in Table 1. An ORTEP diagram[39] for isostructural **1**−**5** is shown in Figure 1. Significant bond geometries for **2**, **3**, and **4** are given in Tables 2 and 3. Complete crystallographic details for **2**, **3**, and **4** are given in the Supporting Information.

Optical Characterization. The infrared emission spectra were recorded by exciting the powdered sample with 980 nm band of a laser diode in the 45° excitation geometry. Emission from the sample was focused onto a 1 m monochromator (Triax 550, Jobin Yvon, Edison, NJ) and detected by a thermoelectrically cooled InGaAs detector (EO Systems, Phoenixville, PA). The signal was intensified with a lock-in amplifier (SR 850 DSP, Stanford Research System, Sunnyvale, CA) and processed by

(36) *SADABS*, v2.05; Bruker Nonius area detector scaling and absorption correction; Bruker-AXS Inc.: Madison, Wisconsin, 2003.
(37) Sheldrick, G. M. *SHELXS86*; Program for the Solution of Crystal Structures; University of Göttingen: Germany, 1986.
(38) Sheldrick, G. M. *SHELXL97*; Program for Crystal Structure Refinement; University of Göttingen: Germany, 1997.
(39) (a) Johnson, C. K. *ORTEP II*, Report ORNL-5138; Oak Ridge National Laboratory: Oak Ridge, TN, 1976. (b) Sheldrick, G. M. *SHELXTL (XP)*, version 6.14; Bruker-AXS, Inc.: Madison, Wisconsin, 2000.

Table 2. Significant Bond Lengths[a] (Å) for **2**, **4**, and **3**

bond	**2**(Er/Hg)	**4**(Yb/Hg)	**3**(Yb/Cd)	bond	**2**(Er/Hg)	**4**(Yb/Hg)	**3**(Yb/Cd)
M(1)−Se(5)	2.520(1)	2.517(1)	2.549(1)	Ln(1)−Se(3)′	2.8284(9)	2.8037(8)	2.772(1)
M(1)−Se(3)	2.578(1)	2.5698(9)	2.619(1)	Ln(2)−N(4)	2.464(9)	2.444(8)	2.435(9)
M(1)−Se(1)	2.7040(9)	2.7063(8)	2.659(1)	Ln(2)−N(3)	2.525(7)	2.504(6)	2.494(8)
M(1)−Se(2)	2.9696(9)	2.9711(8)	2.762(1)	Ln(2)−Se(1)	2.756(1)	2.7380(9)	2.751(1)
Ln(1)−N(2)	2.446(7)	2.420(6)	2.408(7)	Ln(2)−Se(3)	2.8223(9)	2.8055(8)	2.782(1)
Ln(1)−N(1)	2.483(8)	2.461(7)	2.440(8)	Ln(2)−Se(4)	2.833(1)	2.8168(9)	2.813(1)
Ln(1)−Se(1)	2.8012(9)	2.7798(8)	2.779(1)	Ln(2)−Se(2)′	2.8352(9)	2.8082(8)	2.833(1)
Ln(1)−Se(2)	2.8061(9)	2.7865(8)	2.811(1)	Se(4)−C(21)	1.94(1)	1.92(1)	1.95(1)
Ln(1)−Se(2)′	2.8077(10)	2.7904(9)	2.817(1)	Se(5)−C(27)	1.93(1)	1.914(8)	1.91(1)

[a] Symmetry transformations used to generate equivalent atoms: ′ $-x, -y+2, -z$, ″ $-x+1, -y+2, -z$, ‴ $-x, -y+1, -z+1$.

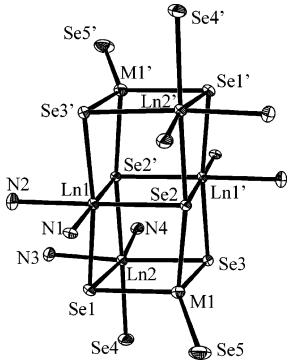

Figure 1. Molecular structure of the hexanuclear heterometallic clusters **1**−**5** with the C and H atoms removed for clarity, and thermal ellipsoids drawn at the 50% probability level for **1**.

computer using Spectramax software (GRAMS 32, Salem, NH). The luminescence lifetime of the infrared emission was measured by the same laser modulated by a mechanical chopper, and the signals were collected by a digital oscilloscope (HP 54520A, 500 MHz, Hewlett-Packard Instruments, Santa Clara, CA). For comparison, both measurements are done at the same experimental configuration. The optical gain coefficient of the powdered samples was measured by the amplified spontaneous emission (ASE) technique in the $L - L/2$ configuration. In ASE, the emission intensity from different lengths of the pumped region of the sample are compared. Commonly, the comparison is made for two discrete values of the pumped length ($L - L/2$) method[40] by masking the pumped beam with a shutter.

Results

Compounds with the hexametallic formulation $(py)_8Ln_4M_2Se_6(SePh)_4$ can be isolated for the latter lanthanides (Ln/M = Er/Cd (**1**), Er/Hg (**2**), Yb/Cd (**3**), Yb/Hg (**4**), Lu/Hg (**5**)) via redox reactions of metal chalcogenolates with elemental Se (reaction 1). Structural characterization of this series of compounds series reveals that they are isostructural, adopting a "double cubane structure". An ORTEP diagram for the structure common to **1**−**5** is given in Figure 1, with significant bond lengths for **2**−**4** given in Table 2 and significant angles for **2**−**4** given in Table 3. Compounds **1** and **5** were shown to be isostructural with **2**−**4** by low-temperature unit cell determination. In the structures, the main group element occupies opposing exterior sites of the double cubane, with distorted tetrahedral geometries that would be impossible to achieve at the inner metal positions. The four Ln are distributed as pairs of interior and exterior metal sites, each with octahedral Ln geometries. The interior Ln coordination spheres contain two neutral pyridine donors, two μ_3 Se^{2-}, and two μ_4 Se^{2-}, whereas the exterior Ln coordinate two μ_3 Se^{2-}, and one μ_4 Se^{2-}, two pyridine, and a terminal selenolate ligand.

$$4Ln(SePh)_3 + 2M(SePh)_2 + 6Se \rightarrow (py)_8Ln_4M_2(SePh)_4 + 3PhSeSePh \quad (1)$$

Complete structural characterization of the ErHg (**2**), YbCd (**3**), and YbHg (**4**) compounds allows for direct comparison of the effects of how Ln and M influence structure. Differences within the Cd and Hg compounds are particularly striking, as these two covalent metals often adopt dramatically different coordination spheres because of the facility with which Hg adopts alternative, nontetrahedral geometries.[41−43] The range of M−Se distances in the Hg compounds suggests a considerably weaker interaction between Hg and Se(2) relative to the cadmium analogue, as judged by the Hg−Se^{2-} bond lengths (i.e. in **2**, Hg−Se(1) = 2.7040(9) Å, Hg−Se(3) = 2.578(1) Å, and Hg−Se(2) = 2.9696(9) Å). The Cd compound **3** contains a far narrower range of M−Se^{2-} bond lengths, (2.659(1) Å, 2.619(1) Å, 2.762(1) Å).

Structural perturbations resulting from a change in Ln are far less dramatic: **2** and **4** have essentially identical structural features and bond lengths that decrease upon replacement of Er (ionic radius = 0.89 Å) with Yb (ionic radius = 0.87 Å).[44] Both Yb compounds crystallize with trace percentages of an additional Se atom inserted into the Yb−Se(Ph) bond.

The materials decompose thermally to give ternary solid-state materials. Slow heating of both Cd compounds **1** and **3** to 650 °C, followed by X-ray powder diffraction analysis of the nonvolatile solid-state product (Figure 2), indicates that $CdLn_2Se_4$ (Ln = Er,[45] Yb[46]) is the only crystalline material present (reaction 2). Analysis of the volatile components with GC/MS identified pyridine and Ph_2Se elimination products. Also, in the Yb thermolysis trace Se_2Ph_2 was detected, the presence of which may be related either to the redox properties of Yb or to the presence of trace Se insertion into a Yb−SePh linkage.

$$(py)_8Ln_4Cd_2Se_6(SePh)_4 \rightarrow CdLn_2Se_4 + 2PhSePh + 8py \quad (2)$$

The $Er_4M_2Se_6$ compounds are highly emissive. A representative absorption spectrum of **1** is shown in Figure 3, revealing the characteristic absorption bands of Er^{3+} originating from $^4I_{15/2}$

(40) Shank, C. V. *Rev. Mod. Phys.* **1975**, *47*, 649.
(41) Bowmaker, G. A.; Dance, I. G.; Harris, R. K.; Henderson, W.; Laban, I.; Scudder, M. L.; Oh, S.-W. *J. Chem. Soc., Dalton Trans.* **1996**, 2381.
(42) Bowmaker, G. A.; Dance, I. G.; Dobson, B. C.; Rogers, D. A. *Aust. J. Chem.* **1984**, *37*, 1607.
(43) Henkel, G.; Krebs, B. *Chem. Rev.* **2004**, *104*, 801.
(44) Shannon, R. D. *Acta Crystallogr., Sect. A* **1976**, *32*, 751.
(45) Fujii, H.; Tetsuhiko, O.; Takahiko, K. *J. Phys. Soc. Jpn.* **1972**, *32*, 1432.
(46) Fujii, H.; Takahiko, K. *Phys. Chem. A* **1972**, *36*, 67.

Table 3. Significant Angles (deg) for **2**, **4**, and **3**

	2(Er/Hg)	**4**(Yb/Hg)	**3**(Yb/Cd)		**2**(Er/Hg)	**4**(Yb/Hg)	**3**(Yb/Cd)
Se(5)−M(1)−Se(3)	138.97(4)	140.05(3)	129.97(5)	N(3)−Ln(2)−Se(3)	173.8(2)	173.5(2)	175.0(2)
Se(5)−M(1)−Se(1)	108.91(3)	109.05(3)	113.69(4)	Se(1)−Ln(2)−Se(3)	98.72(3)	98.86(3)	96.90(3)
Se(3)−M(1)−Se(1)	106.52(3)	105.88(3)	103.34(4)	N(4)−Ln(2)−Se(4)	94.1(2)	85.0(2)	84.5(2)
Se(5)−M(1)−Se(2)	101.42(3)	101.51(3)	108.38(4)	N(3)−Ln(2)−Se(4)	90.4(2)	88.5(2)	87.8(2)
Se(3)−M(1)−Se(2)	94.77(3)	94.05(2)	96.93(3)	Se(1)−Ln(2)−Se(4)	92.30(3)	89.26(3)	88.50(3)
Se(1)−M(1)−Se(2)	95.97(3)	95.08(2)	99.37(3)	Se(3)−Ln(2)−Se(4)	92.00(3)	89.55(2)	89.51(3)
N(2)−Ln(1)−N(1)	84.4(3)	84.5(2)	85.8(3)	N(4)−Ln(2)−Se(2)′	84.3(2)	93.8(2)	93.8(2)
N(2)−Ln(1)−Se(1)	85.98(19)	86.16(16)	87.2(2)	N(3)−Ln(2)−Se(2)′	87.9(2)	90.4(2)	90.7(2)
N(1)−Ln(1)−Se(1)	90.4(2)	90.3(2)	90.5(2)	Se(1)−Ln(2)−Se(2)′	89.03(3)	91.74(3)	93.05(4)
N(2)−Ln(1)−Se(2)	171.8(2)	171.6(2)	173.5(2)	Se(3)−Ln(2)−Se(2)′	89.53(3)	91.46(3)	91.93(3)
N(1)−Ln(1)−Se(2)	88.2(2)	88.1(1)	88.2(2)	Se(4)−Ln(2)−Se(2)′	177.79(3)	178.45(3)	177.74(4)
Se(1)−Ln(1)−Se(2)	97.61(3)	97.73(2)	95.41(3)	M(1)−Se(1)−Ln(2)	76.87(3)	77.00(2)	79.82(3)
N(2)−Ln(1)−Se(2)′	95.4(2)	95.33(16)	94.4(2)	M(1)−Se(1)−Ln(1)	85.19(3)	85.63(2)	83.56(3)
N(1)−Ln(1)−Se(2)′	179.1(2)	179.1(2)	178.7(2)	Ln(2)−Se(1)−Ln(1)	91.54(3)	91.32(2)	92.53(3)
Se(1)−Ln(1)−Se(2)′	88.69(3)	88.78(3)	88.29(3)	Ln(1)−Se(2)−Ln(1)′	87.96(3)	87.81(2)	88.43(3)
Se(2)−Ln(1)−Se(2)′	92.04(3)	92.19(2)	91.58(3)	Ln(1)−Se(2)−Ln(2)′	90.23(3)	90.25(2)	89.18(3)
N(2)−Ln(1)−Se(3)′	86.2(2)	85.9(2)	87.2(2)	Ln(1)′−Se(2)−Ln(2)′	89.77(3)	89.65(2)	89.99(3)
N(1)−Ln(1)−Se(3)′	87.8(2)	87.7(2)	89.0(2)	Ln(1)−Se(2)−M(1)	80.31(2)	80.66(2)	81.12(3)
Se(1)−Ln(1)−Se(3)′	172.13(3)	171.93(2)	174.37(3)	Ln(1)′−Se(2)−M(1)	81.68(3)	81.85(2)	82.86(3)
Se(2)−Ln(1)−Se(3)′	90.00(3)	90.03(2)	90.18(3)	Ln(2)′−Se(2)−M(1)	167.42(4)	167.74(3)	168.07(4)
Se(2)′−Ln(1)−Se(3)′	93.08(3)	93.16(2)	92.26(3)	M(1)−Se(3)−Ln(1)′	88.60(3)	89.19(3)	86.41(3)
N(4)−Ln(2)−N(3)	84.7(3)	84.8(2)	84.9(3)	M(1)−Se(3)−Ln(2)	77.74(3)	78.04(2)	79.94(3)
N(4)−Ln(2)−Se(1)	169.5(2)	170.3(2)	169.6(2)	Ln(2)−Se(3)−Ln(1)′	90.05(3)	89.95(2)	91.05(3)
N(3)−Ln(2)−Se(1)	86.9(2)	87.3(2)	87.3(2)	C(21)−Se(4)−Ln(2)	105.7(3)	107.0(3)	106.5(3)
N(4)−Ln(2)−Se(3)	89.4(2)	88.9(2)	90.7(2)	C(27)−Se(5)−M(1)	101.2(3)	101.6(2)	100.3(3)

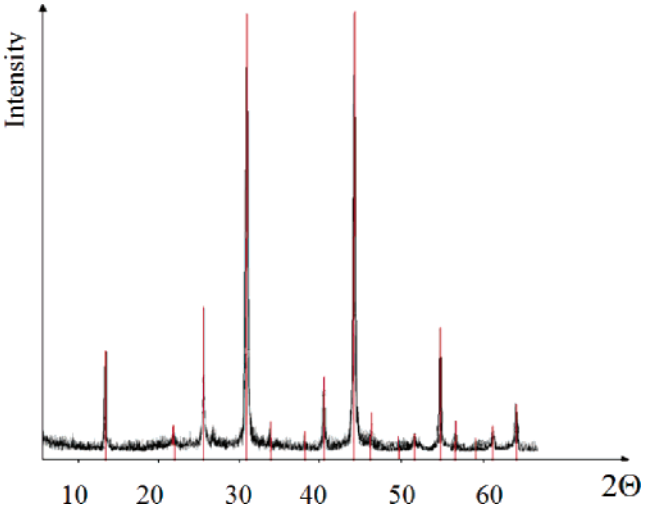

Figure 2. X-ray powder diffraction profile of the solid-state material formed in the pyrolysis of **2**, with the red lines representing the published diffraction profile for $CdEr_2Se_4$.

ground state to various excited states. The emission infrared spectra of the two Er complexes **1** and **3** are shown in Figure 4, along with an inset of the spectrum for $(THF)_{14}Er_{10}S_6(SeSe)_6I_6$.[17] The $^4I_{11/2}$ excited state was populated by 980 nm photons. A part of the excited population decays to $^4I_{13/2}$ by multiphonon relaxation, and the remaining population will appear as radiative decay by the $^4I_{13/2} \rightarrow {}^4I_{15/2}$ channel, which is responsible for the 1542 nm emission. The lifetime of this emission was extracted from an exponential curve fit of the 1542 nm fluorescence decay (see Supporting Information) with values of 1.41 and 0.71 ms, respectively, for **1** and **2**. With this fluorescence decay time, the quantum yield of 1542 nm emission can be estimated from the ratio of the fluorescence decay time (τ_{fl}) to radiative or "natural" decay time (τ_r). With a calculated radiative decay time of 3.85 ms following the Judd−Ofelt procedure,[47,48] quantum efficiencies of 37% (**1**) and 19% (**2**)

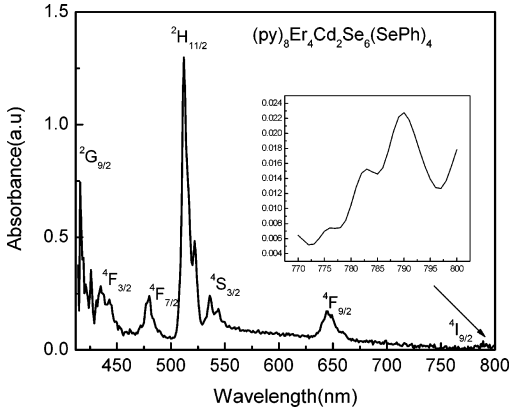

Figure 3. Optical absorption spectrum of $(py)_8Er_4Cd_2Se_6(SePh)_4$ in pyridine. (Inset) NIR absorption band at 800 nm.

are obtained. The fluorescence spectral width (fwhm) and stimulated emission cross section are estimated to be respectively 35 nm, 33 nm ,and 1.68×10^{-20} cm^2, which are comparable to the well-known host LaF_3:Er.[49] The optical gain coefficients obtained are respectively 2.77 and 1.86 cm^{-1} for **1** and **2**.

Discussion

Compounds **1**−**5** represent the first molecular picture of Ln−E−M linkages. They are related morphologically to the lanthanide cubane structures $(py)_8Yb_4Se_4(SePh)_4$,[50] $(THF)_8Yb_6Se_6I_6$,[51] and $(py)_8Yb_6S_6(SPh)_6$,[50] with a $MLnSe_2$ fragment capping one face of a MLn_3Se_4 cubane structure. It is significant that the strong pyridine ligand does not fragment these hexanuclear structures to give, for example, $(py)_8Yb_3MSe_4(SePh)_3$, as was found for $(py)_8Yb_4Se_4(SePh)_4$. Rather, the $Ln_4M_2Se_6$

(47) Judd, B. R. *Phys. Rev. B: Condens. Mater. Phys.* **1962**, *127*, 750.
(48) Ofelt, G. S. *J. Chem. Phys.* **1962**, *37*, 511.
(49) Kumar, G. A.; Ballato, J.; Snitzer, E.; Riman, R. E. *J. Appl. Phys.* **2004**, *95*, *40*.
(50) Freedman, D.; Melman, J. H.; Emge, T. J.; Brennan, J. G. *Inorg. Chem.* **1998**, *37*, 4162.
(51) Kornienko, A.; Emge, T. J.; Hall, G.; Brennan, J. G. *Inorg. Chem.* **2002**, *41*, 121.

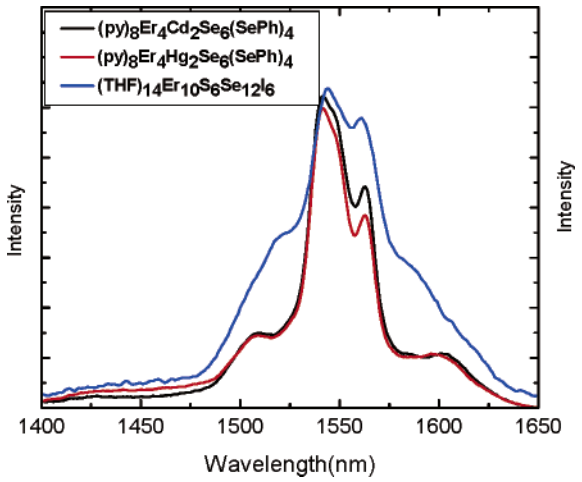

Figure 4. Comparison of the Infrared emission spectra of the $(py)_8Er_4M_4Se_6(SePh)_4$ complexes with $(THF)_{14}Er_{10}S_6Se_{12}I_6$.[17]

framework can be rationalized by assuming that introduction of the divalent M presents a problem in charge balance. If, from past experiments, we can assume that the M will coordinate one SePh to achieve the preferred tetrahedral geometry, then to have the $Ln_3MSe_4(SePh)_3$ formula there would have to be one selenolate-free Ln. Such an exposed, pyridine-saturated Ln would be more prone to oligiomerization. Selenido ligands have adopted double cubane structures before but only when crystallized from the less basic solvent THF, and then only with sterically undemanding ancillary anions that can effectively coordinate inner as well as outer Ln.

Direct comparisons of structural features and bond length distributions within this double cubane family are complicated by the inequivalent distribution of ancillary (EPh, I) ligands in all structures. Iodides coordinate uniformly to both internal and external Ln within the Ln_6 framework, whereas in the thiolate compound the SPh ligands were distributed such that the internal Ln did not coordinate SPh. Comparisons of **3** and **4** with the selenido cluster $(THF)_8Yb_6Se_6I_6$ are particularly relevant, as all have a set of distinctly similar Yb ions that allow for an evaluation of the Ln−Se-M interaction.

Even with these similar coordination environments, bond length comparisons are difficult to make, given the multitude of factors that influence Ln−E bond lengths. For example, it has been noted that in octahedral Ln chalcogenolate and chalcogenido cluster compounds, the identity of the trans-ligand appears to have a slight (ca. 0.02−0.05 Å) but statistically significant influence on Ln−E bond lengths.[50−54] Further, in the structures of $(THF)_6Yb_4E(EE)_4I_2$ (E = S, Se) it was noted that anion distribution influenced Ln−E bond lengths, with the two metals coordinating iodide anions showing greater Ln−E bond lengths than bonds to the two iodide-free Ln.[55] Even with these constraints, there are a pair of direct bond length comparisons within the three Yb selenido cluster compounds **3**, **4**, and $(THF)_{10}Yb_6Se_6I_6$ that reveal how the presence of M influences the length of the $Ln-E^{2-}$ bond.

Looking first at bonds from Yb to the triply bridging Se^2, the two Yb−Se bond lengths trans to a neutral THF ligand in the iodo compound are 2.730(2) and 2.750(2) Å, while the analogous Yb(2)−Se(1)/Yb(2)−Se(3) distances in **3** and **4** are 2.751(1)/2.782(1) and 2.738(1)/2.806(1) Å, respectively. Of the four comparisons, the Yb(2)−Se(1) distance in **4** stands out, but this is easily placed in context by looking at the M−Se bond lengths. In **4**, Cd−Se(3) (2.619(1) Å) is longer than Cd−Se(1) (2.659(1) Å), and in **3**, Hg−Se(1) is significantly longer (2.7063(8) Å) than Hg−Se(3) (2.5698(9) Å). In each set of distances, long Ln−Se(*x*) bonds are correlated with shorter M−Se(*x*) bonds.

An examination of the μ_4 Se^{2-} ligand reveals similar effects. Again, only the most structurally related set of distances are compared. Here, in the iodo compound there is a single Yb−Se bond for which the Yb bonds two neutral donors, an anion (iodide), two μ_3 Se^{2-}, and a μ_4 Se^{2-}. The latter bond length, at 2.817(1) Å, is the longest $Yb-Se^{2-}$ bond in the structure. In comparison, **3** and **4** have one bond, Ln(2)−Se(2′) with bond lengths 2.833 Å for **3** and 2.808 Å for **4**, that, at first glance, appear very similar, with the bond in the Hg compound actually shorter than the iodide, while the bond in the Cd compound is slightly longer than the iodide. A look at the M−Se(2) distance is again revealing, for in the Hg compound Hg−Se(2) is almost 0.3 Å longer than either Cd−Se(2) or the other Hg−Se bonds. Again, Ln−Se bond lengths appear to increase as Hg−Se bond lengths become shorter. These distortions are significantly less dramatic than similar perturbations noted in heterometallic selenolate structures,[56−59] as might be expected, given that the $Ln-Se^{2-}$ bond should be less easily distorted than its Ln−Se-$(Ph)^-$ counterpart.

Identification of the thermolysis products of $(py)_8Ln_4Cd_2Se_6(SePh)_4$ clusters is important because these molecules can be sources for low-temperature syntheses of heterometallic solid-state materials. Two compounds, $(py)_8Yb_4Cd_2Se_6(SePh)_4$ and $(py)_8Er_4Cd_2Se_6(SePh)_4$ were decomposed, and X-ray powder diffraction profiles of the resultant solid-state product indicated that $CdYb_2Se_4$[46] and $CdEr_2Se_4$[45] were the only crystalline solid phases present. The decomposition proceeds in stages, with pyridine dissociation occurring at room temperature and the organoselenium products eliminating at elevated temperatures. Analysis of the organic products by GC/MS identified $SePh_2$ as the Ph-containing products in both experiments. While ternary materials have been prepared in this fashion (both alloys[60−62] and compounds with well-defined M/M′ lattice positions),[63−65] the present compounds are distinctive in their combination of such dissimilar metals.

Maintenance of this heterometallic distribution throughout the thermolysis experiment contrasts with earlier attempts to prepare

(52) Lee, J.; Brewer, M.; Berardini, M.; Brennan, J. *Inorg. Chem.* **1995**, *34*, 3215.
(53) Geissinger, M.; Magull, J. *Z. Anorg. Allg. Chem.* **1995**, *621*, 2043.
(54) Mashima, K.; Nakayama, Y.; Fukumoto, H.; Kanehisa, N.; Kai, Y.; Nakamura, A. *J. Chem. Soc., Chem. Commun.* **1994**, 2523.
(55) Melman, J.; Fitzgerald, M.; Freedman, D.; Emge, T.; Brennan, J. G. *J. Am. Chem. Soc.* **1999**, *121*, 10247.
(56) Freedman, D.; Emge, T. J.; Brennan, J. G. *J. Am. Chem. Soc.* **1997**, *119*, 11112.
(57) Lee, J.; Emge, T.; Brennan, J. *Inorg. Chem.* **1997**, *36*, 5064.
(58) Berardini, M.; Emge, T.; Brennan, J. *Inorg. Chem.* **1995**, *34*, 5327.
(59) Berardini, M.; Emge, T.; Brennan, J. *J. Am. Chem. Soc.* **1994**, *116*, 6941.
(60) DeGroot, M. W.; Taylor, N. J.; Corrigan, J. F. *J. Am. Chem. Soc.* **2003**, *125*, 864.
(61) DeGroot, M. W.; Corrigan, J. F. *Angew. Chem., Int. Ed.* **2004**, *43*, 5355.
(62) DeGroot, M. W.; Taylor, N. J.; Corrigan, J. F. *J. Mater. Chem.* **2004**, *14*, 654.
(63) Goel, S. C.; Buhro, W. E.; Adolphi, N. L.; Conradi, M. S. *J. Organomet. Chem.* **1993**, *449*, 9.
(64) Jin, M. H.; Banger, K. K.; Harris, J. D.; Hepp, A. F. *Mater. Sci. Eng., B* **2005**, *B116*, 395.
(65) Deivaraj, T. C.; Park, J.; Afzaal, M.; O'Brien, P.; Vittal, J. J. *Chem. Mater.* **2003**, *15*, 2383.

ternary solid-state compounds from molecular chalcogenolate compounds, which decomposed to deliver phase-separated Ln and M solids. While $Ln(ER)_x$ react with $M(ER)_2$ to form heterometallic compounds in quantitative yields, the driving force behind this reactivity apparently did not survive the thermolysis process. These heterometallic compounds decomposed to give phase-separated solids, i.e., EuS and MS from $EuM(SPh)_4$ (M = Zn, Cd),[66] or in the case of Hg, LnE with the elimination of volatile $Hg(SPh)_2$. Characterization of the heterocluster salt $[(THF)_8Sm_4Se(SePh)_8][Zn_8Se(SePh)_{18}]$[35] supported the view that these compounds were destined to deliver LnE and ME phases, by revealing a molecular picture of the initial step in phase separation. The present work is significant in demonstrating the ability to prepare ternary Ln/M solids from molecular precursors, as long as the component metals are present in the initial thermolysis precursor.

Electronic spectra can also be used to evaluate the influence of M upon the Ln−Se bond. The Er and Lu compounds are both yellow, indicating that any Se-to-M charge transfer (CT) absorption is still primarily in the UV spectrum and tails into the visible spectrum. The Yb compounds are intensely red due to the presence of a Se-to-Yb charge-transfer absorption at 410 nm in 4-ethylpyridine. In divalent molecular chalcogenolate studies the Ln-to-pyridine charge-transfer excitation energies were interpreted in terms of M polarizing EPh electron density away from the Ln.[67] The present systems can be examined similarly, although it should be noted early that in trivalent systems Se-to-Ln charge-transfer absorptions in chalcogenido clusters are rarely well defined due to the presence of so many different E and Ln within a given product. Of the Yb with selenium ligands, Se-to-Yb charge-transfer absorptions have been resolved only for $Yb(SePh)_3$ (λ_{max} = 510 nm).[52] In the electronic spectrum of **3** and **4** there is an absorption maximum at 440 nm that can comfortably be assigned[68] as a Se-to-Yb charge-transfer excitation. The relatively high energy of LMCT absorptions in **3** and **4** would be consistent with an increased stabilization of Se electron density upon coordination to M.

As in the case of $(THF)_{14}Er_{10}S_6(SeSe)_6I_6$ the Er atoms in **1** and **2** are bonded in an environment where heavy atoms are the strongly bonded set of neighbors and nearest neighbors, and hence similar radiative properties can be expected. Fluorescence decay times of 1.41 and 0.71ms are obtained for **1** and **2** respectively, as is often found for solid-state Er ions coordinated by selenide, sufide, or iodide, where lifetimes ranges from 2.3 to 4 ms.[14,69,70] The present decay rates contrast with those of more conventional molecular complexes of Er that are typically in the microsecond range[71,72] characteristic of high phonon energy materials. Comparison of the effective emission spectral bandwidth of **1** and **2** with that of Er_{10} shows a 45% reduction in the Er/M compounds that can be attributed to the lower inhomogeneous broadening associated with a lesser number of Er atoms in the lattice locations.

Excited-state lifetimes for **1** and **2** are significantly shorter than in the case of $(THF)_{14}Er_{10}S_6(SeSe)_6I_6$. Intermetallic Er−Er distances in **1** and **2** are essentially identical to Er−Er distances in the Er_{10} cluster: within each molecule, distances from the inner Er to the inner and to the two outer Er (**1**: 3.94, 3.99, 4.02 Å. **2**: 3.90, 3.98, 4.00 Å) are not significantly different from the smallest set of distances separating Er in the Er_{10} cluster; thus, concentration quenching is not the dominant variable determining emission intensity.

Presumably, then, it is the abundance of anionic SeC_6H_5 ligands attached to Er (and M) in **1** and **2** that are influencing relaxation properties. In Er^{3+} compounds one of the principle channels of multiphonon nonradiative decay is via $^4I_{11/2} \rightarrow {}^4I_{13/2}$, which is in the frequency region of 3700 cm^{-1}. Typically for chalcogenides the highest vibrational frequency is ca. 700 cm^{-1}; thus, at least five phonons are required to bridge the $^4I_{11/2} \rightarrow {}^4I_{13/2}$ energy gap, and the probability of such a higher order process is limited. Thus, nonradiative relaxation by such multiphonon process can be neglected. Similarly, population of the $^4I_{13/2}$ state during the $^4I_{13/2} \rightarrow {}^4I_{15/2}$ decay can be further lost by vibrational groups of frequency 6500 cm^{-1}. The second-order vibrational energy of C−H (2960 cm^{-1}) is resonant with the Er^{3+} first excited state (6500 cm^{-1}), and thus Er^{3+} directly attached to any of these vibrational groups or their harmonics will experience higher nonradiative loss with diminished quantum efficiency, as observed in all reported molecular Er complexes reported to date. In contrast to the Er_{10} cluster, both **1** and **2** have anionic ligands with C−H functionalities, and these may be contributing to nonradiative relaxation of the excited state. These observations are important in the rational design of emissive materials with optimal performance.

Conclusion

Heterometallic clusters containing Ln and M connected by chalcogenido ligands are synthetically viable targets. Covalently bonded M polarize E electron density away from Ln, thus increasing Ln−E bond lengths. The Ln/Cd compounds decompose thermally to give ternary solid-state materials. In the case of Er, these compounds are highly emissive, with intensities that depend on M and appear to be impacted adversely by the presence of SePh ligands.

Acknowledgment. This work was supported by the National Science Foundation under Grant No. CHE-0303075, the New Jersey State Commission on Science and Technology, and the APEX diffractometer was obtained under Grant CHE-0091872.

Supporting Information Available: X-ray crystallographic files in CIF format for the crystal structures of **2**−**4**. This material is available free of charge via the Internet at http://pubs.acs.org.

JA0534708

(66) Brewer, M.; Emge, T.; Brennan, J. *Inorg. Chem.* **1995**, *34*, 5919.
(67) Brewer, M.; Khasnis, D.; Buretea, M.; Berardini, M.; Emge, T. J.; Brennan, J. G. *Inorg. Chem.* **1994**, *33*, 2743.
(68) Lee, J.; Freedman, D.; Melman, J.; Brewer, M.; Sun, L.; Emge, T. J.; Long, F. H.; Brennan, J. G. *Inorg. Chem.* **1998**, *37*, 2512.
(69) Fick, J.; Knystautas, E. J.; Villeneuve, A.; Schiettekatte, A.; Roorda, S.; Richardson, K. A. *J. Non-Cryst. Solids* **2000**, *272*, 200.
(70) Ye, C. C.; Hewak, D. W.; Hempstead, M.; Samson, M.; Payne, D. N. *J. Non-Cryst. Solids* **1996**, *208*, 56.
(71) Washburn, B. R.; Diddams, S. A.; Newbury, N. R.; Nicholson, J. W.; Yan, M. F.; Jorgensen, C. G. *Opt. Lett.* **2004**, *29*, 250.
(72) Yiannopoulos, K.; Vyrsokinos, K.; Tsiokos, D.; Kehayas, E.; Pleros, N.; Theophilopoulos, G.; Houbavlis, T.; Guekos, G.; Avramopoulos, H. *IEEE J. Quantum Elect.* **2004**, *40*, 157.